Acta Med. Okayama, 2015
Vol. 69, No. 3, pp. 165–171

Acta Medica Okayama
http://escholarship.lib.okayama-u.ac.jp/amo/

Original Article

Dynamic Finite Element Analysis of Impulsive Stress Waves Propagating from the Greater Trochanter of the Femur by a Sideways Fall

Takaaki Sarai[a]* and Akihiro Tokumoto[b]

[a]Division of Industrial Innovation Sciences, Graduate School of Natural Science and Technology, Okayama University, Okayama 700–8530, Japan, and [b]Fujikura Co., Ltd., Chiba 285–8550, Japan

Fall accidents are a common cause of femoral fracture in the elderly. The greater trochanter of the femur is often subjected to impact loading by a sideways fall, and thus it is worth studying the impulsive stress waves propagating in the femur. In this study, the impulsive stress was analyzed by the dynamic finite element method using a 3-dimensional model of the femur, and the influence of the fall configuration on the stress was discussed. The stress was concentrated around the femoral neck during the propagation of the stress wave, and the tensile maximum principal stress changed into compressive minimum principle stress on the anterior and medial sides of the neck. On the other hand, the compressive minimum principal stress changed into tensile maximum principle stress on the lateral side of the neck. The largest maximum principal stress during the impact loading was always larger in the neck than in the impact region. The largest absolute value of the minimum principal stress was found in the neck or the impact region depending on the fall configuration. The largest absolute values of the maximum and minimum principal stress were nearly equal, indicating that the bone fracture due to the tensile stress may occur around the femoral neck.

Key words: biomechanics, sideways fall, femoral neck, greater trochanter, impulsive stress wave

Computational biomechanics is a very important approach for clarifying the various behaviors of the human body, and finite element analysis is considered to be one of the most useful methods for computational biomechanics. Many studies have analyzed the biomechanics of the femur using the finite element method [1–14], and in our previous paper [15], we also examined the impulsive stress waves propagating from the distal end of the femur. Femoral fracture in the elderly mainly occurs due to a blow to the greater trochanter by a sideways fall, and therefore the bone strength of the proximal femur subjected to a sideways fall has been estimated analytically in biomechanical studies [4, 12]. Quality of life is greatly impaired in individuals bedridden due to bone fracture, so it is important to find new ways for preventing fall accidents, particularly in the current context of an aging society. An important aspect of this research is evaluating impulsive stress in the femur and determining changes in the stress state during propagation of stress waves.

Received August 7, 2014; accepted January 16, 2015.
*Corresponding author. Phone:+81–86–251–8030; Fax:+81–86–251–8266
E-mail:sarai@mech.okayama-u.ac.jp (T. Sarai)

Conflict of Interest Disclosures: No potential conflict of interest relevant to this article was reported.

In the present work, the impulsive stress waves propagating from the greater trochanter after a sideways fall were analyzed using a 3-dimensional model of the femur created in our previous study [15]. The dynamic finite element method was employed and the propagation of the stress wave was discussed in relation to the fall configuration. The purpose of this study was to evaluate the impulsive stress causing femoral fracture after a sideways fall, and to determine where the greatest stress is concentrated in the femur.

Materials and Methods

The finite element model was constructed and described in detail in our previous study [15]. The CT images of the right femur of an adult man were prepared and the contour lines of the cortical bone and the cancellous bone were extracted from them. The solid model was then created and divided into 13,780 4-node tetrahedral elements with 3,305 nodes. The model consisted of the cortical bone and the cancellous bone, and was approximately 414 mm in total length. The isotropic properties of the bones were assumed in the analysis and the material constants for the elastic deformation were taken from the data book [16], as in the previous analysis [15]; the elastic modulus, Poisson's ratio, and density of the cortical bone were 7GPa, 0.3, and 1,700 kg/m^3, and those of the cancellous bone were 1GPa, 0.3, and 1,100 kg/m^3, respectively.

A rigid surface was set horizontally and the lateral fall configuration was defined by the 2 angles shown in Fig. 1; θ is the angle in the sagittal plane between the bone axis of the femur and the surface, and ϕ is the inclination angle of the femur from the vertical direction. It was assumed that the femur is separated from the pelvis by the articular cartilage; the trunk drawn in the figure is not concerned with the analysis. The angles used in the analysis were $\theta = 10$, 20, and 30 degrees and $\phi = 45$, 60, and 75 degrees for a sideways fall. Fig. 2 shows the positional relation between the femur and the rigid surface in the cases of $\theta = 20°$, $\phi = 45$, 60, and 75 degrees. The impact was applied in the vertical direction by hitting the greater trochanter against the surface attached to the several element surfaces including the lowest node of the model. The impact region is shown as the black element surfaces in Fig. 2 for each inclination angle.

The impact velocity was set at 1 m/sec for each fall configuration and the displacements of the nodes facing the rigid surface were fixed in the horizontal plane, perpendicular to the impact direction, for stable impact. The propagation of the stress wave was analyzed by the software MSC.Marc 2008 (MSC.Software) employing the dynamic explicit method until the elapsed time $t = 500$ μsec at the time intervals of $\Delta t = 5 \times 10^{-8}$ sec.

Results

The von Mises equivalent stress distributions of the cortical bone surface in the lateral view of the femur are shown in Fig. 3; the results for $\theta = 20°$, $\phi = 60°$ at $t = 100$, 200, 300, 400, 500 μsec are represented in the figure. The stress wave propagated from the greater trochanter and eventually reached the femoral

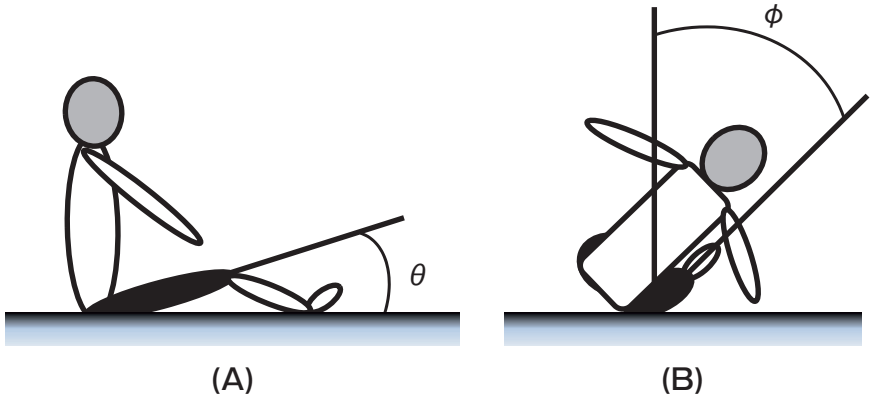

Fig. 1 Sideways fall configuration. θ is the angle in the sagittal plane between the bone axis of the femur and a horizontal rigid surface (A). ϕ is the inclination angle of the femur from the vertical direction (B).

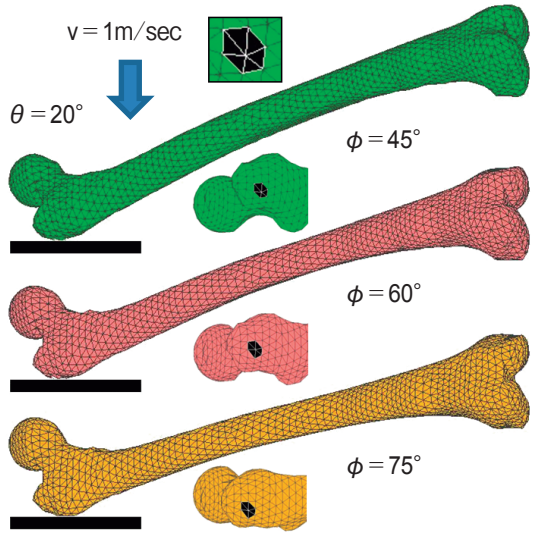

Fig. 2 Positional relation between the femur and a rigid surface in the cases of $\theta = 20°$, $\phi = 45$, 60, and 75 degrees. Black element surfaces show the impact region, *i.e.*, the position of impact of the greater trochanter, for each inclination angle.

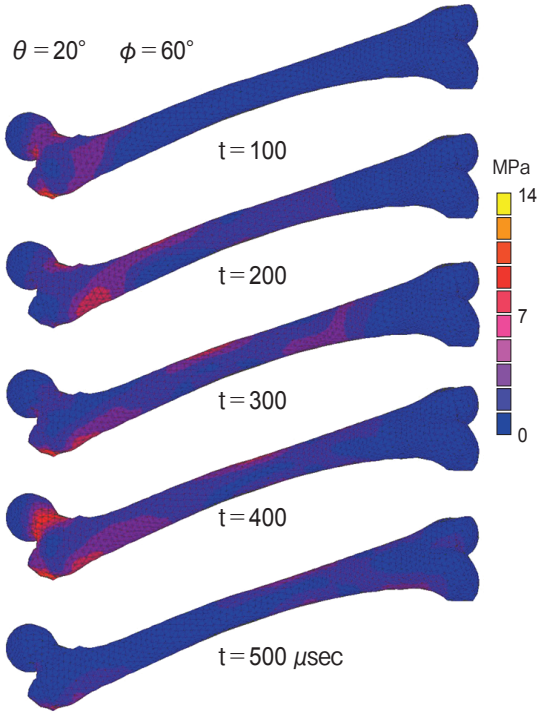

Fig. 3 Propagation of the stress wave in the cortical bone surface of the femur in the case of $\theta = 20°$, $\phi = 60°$. Distributions of the equivalent stress in the lateral view of the femur at $t = 100$, 200, 300, 400, 500 μsec are shown.

neck, diaphysis, and distal femur.

Large equivalent stress was observed around the femoral neck during the propagation of the stress wave, as shown in Fig. 3. The change of the stress in the cortical bone surface around the cross section of the neck was evaluated; the time histories of the equivalent stress of the nodes located on the anterior, posterior, medial, and lateral sides of the neck in the cases of $\theta = 20°$, $\phi = 45$, 60, and 75 degrees are shown in Fig. 4. The change of the stress differed according to the location around the neck. The stress on each side increased and decreased twice until $t = 500$ μsec and became very small at around $t = 260$ μsec. The stress on the lateral side was largest, and was much greater than the stress on the other sides.

The large equivalent stress was observed twice in Fig. 4, so the distributions of the maximum and minimum principal stress of the cortical bone surface in the proximal femur at $t = 100$, 400 μsec in the case of $\theta = 20°$, $\phi = 60°$ are shown from two different viewpoints in Fig. 5. The maximum principal stress was concentrated on the medial side at $t = 100$ μsec and on the lateral side at $t = 400$ μsec, respectively. On the other hand, the absolute value of the minimum princi-

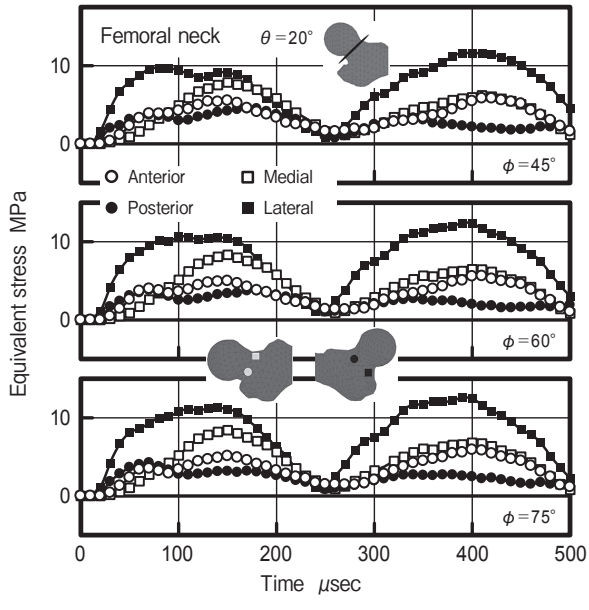

Fig. 4 Time history of the equivalent stress in the cortical bone surface around the femoral neck in the cases of $\theta = 20°$, $\phi = 45$, 60, and 75 degrees. Changes of the stress with the elapsed time were evaluated for 4 nodes located around the cross section of the femoral neck shown in the Figure.

pal stress became large on the lateral side at t = 100 μsec and on the medial side at t = 400 μsec. The distributions of the maximum and minimum principal stress in the inclined cross section are shown in Fig. 6, in correspondence with the data in Fig. 5. A large absolute value of the principal stress was found in the cortical bone, and the value was small in the internal cancellous bone.

Fig. 7A shows the time histories of the maximum and minimum principal stress around the femoral neck in the case of θ = 20°, ϕ = 60°, where the reference nodes are the same 4 nodes used in Fig. 4. Fig. 7B presents similar results in the impact region for θ = 20°, ϕ = 45, 60, and 75 degrees. Within the impact region, the node having the largest absolute value of the maximum or minimum principal stress during the impact loading was chosen for each ϕ. The maximum principal stress increased at the beginning of the propagation, and after that the absolute value of the minimum one increased on the anterior and medial sides of the neck. In contrast, the absolute value of the minimum principal stress increased at first and then the maximum one became large on the lateral side. The largest absolute values of the maximum and minimum principal stress during the propagation were larger on the lateral side than on the medial side. The pattern of change in the stress in the impact region was simpler than that in the neck. The absolute value of the minimum principal stress increased until at around t = 100 μsec and the maximum one became large at around t = 400 μsec. The minimum principal stress in the impact region differed according to the inclination angle.

As shown in Fig. 7A, the principal stress on the

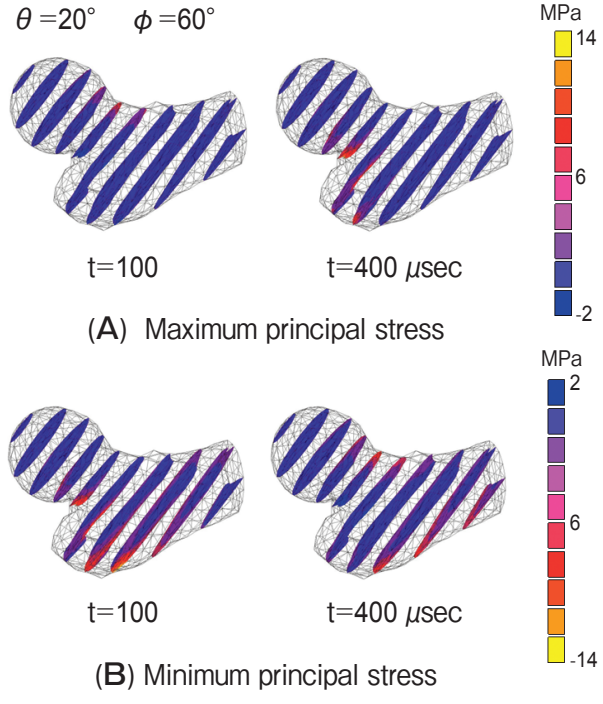

Fig. 6 Distributions of the maximum (**A**) and minimum (**B**) principal stress in the inclined cross section of the proximal femur in the cases of θ = 20°, ϕ = 60° at t = 100, 400 μsec; these data correspond to those in Fig. 5.

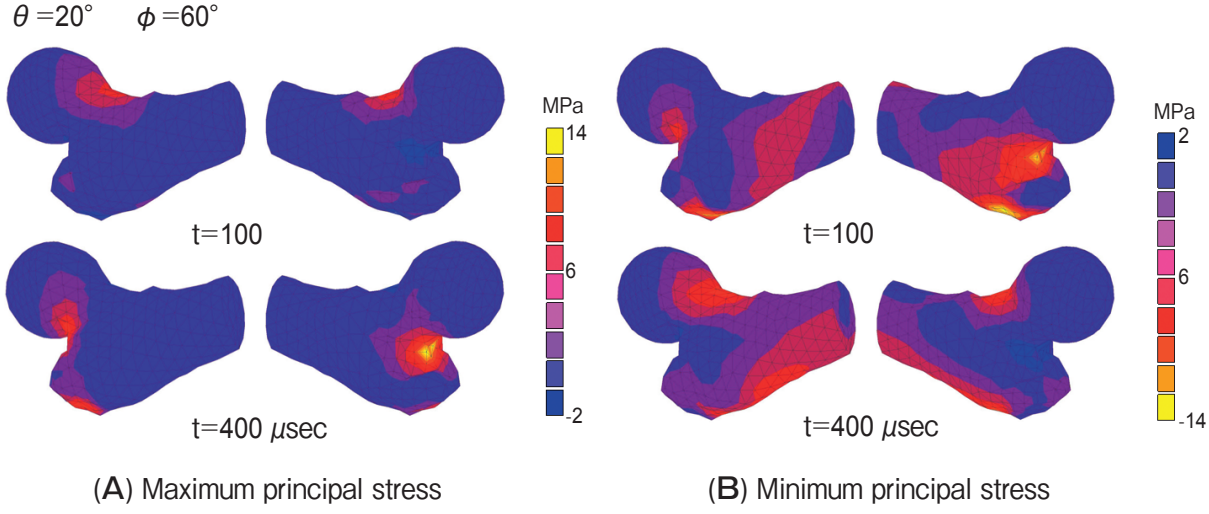

Fig. 5 Distributions of the maximum (**A**) and minimum (**B**) principal stress in the cortical bone surface of the proximal femur in the cases of θ = 20°, ϕ = 60° at t = 100, 400 μsec.

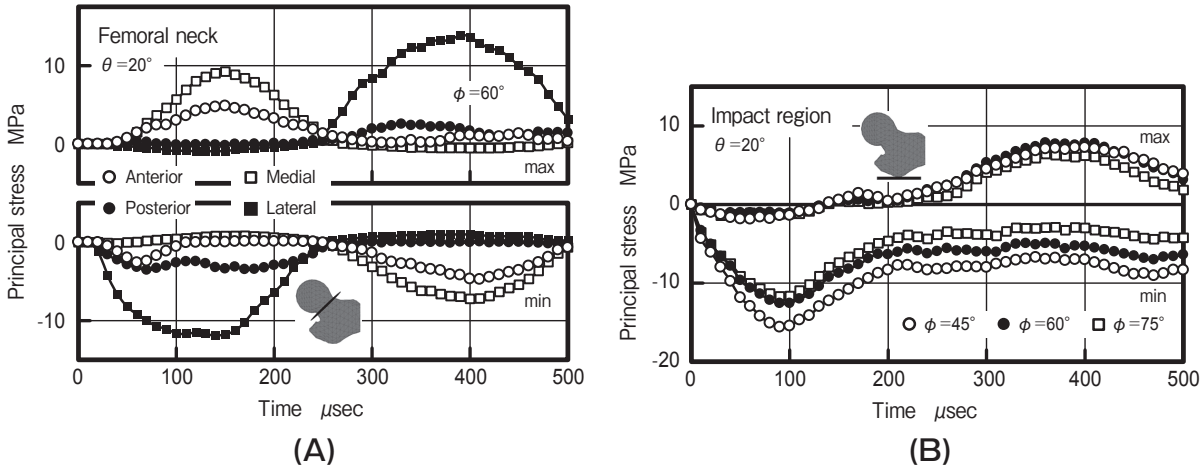

Fig. 7 Time history of the principal stress in the cortical bone surface around the femoral neck in the case of $\theta = 20°$, $\phi = 60°$ (A) and that in the impact region in the cases of $\theta = 20°$, $\phi = 45$, 60, and 75 degrees (B).

anterior, posterior, medial, and lateral sides of the femoral neck fluctuated with the elapsed time. The largest absolute values of the maximum and minimum principal stress during the impact loading were evaluated on the 4 sides around the neck. Fig. 8 shows the relation between these largest values and the inclination angle in the case of $\theta = 20°$. The absolute value of the principal stress was largest on the lateral side and was small on the anterior and posterior sides for any inclination angle.

Fig. 9 shows the largest absolute values of the maximum and minimum principal stress in the femoral neck area and the impact region during the impact loading; the values are plotted against θ for each inclination angle. The area of the neck used for the stress evaluation is represented in the figure and the largest absolute values were obtained by the time histories in this area. The influence of θ was relatively small and the absolute values of the principal stress increased as ϕ increased in the neck. In this case, the maximum principal stress was a little larger than the absolute value of the minimum one for the same fall configuration. The maximum principal stress was larger in the neck than in the impact region for every fall configuration. The minimum principal stress in the impact region was affected by the inclination angle, and the absolute value for $\phi = 45°$ was larger than the values for $\phi = 60$ and 75 degrees. The absolute value of the minimum principal stress for $\phi = 45°$ was larger in the impact region than in the neck, especially in the case of $\theta = 30°$.

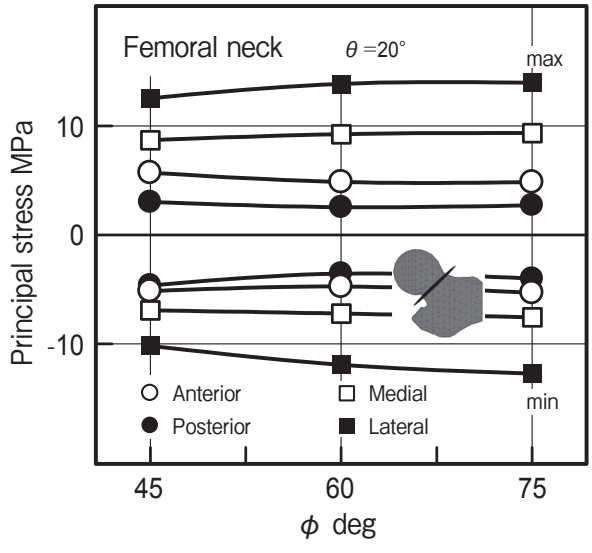

Fig. 8 The largest absolute values of the maximum and minimum principal stress in the cortical bone surface around the femoral neck during the propagation of the stress wave ($t = 0-500$ μsec). The relation between the largest values and the inclination angle in the case of $\theta = 20°$ is shown.

Discussion

The equivalent stress around the femoral neck increased and decreased twice and became very small on every side at around $t = 260$ μsec. Corresponding

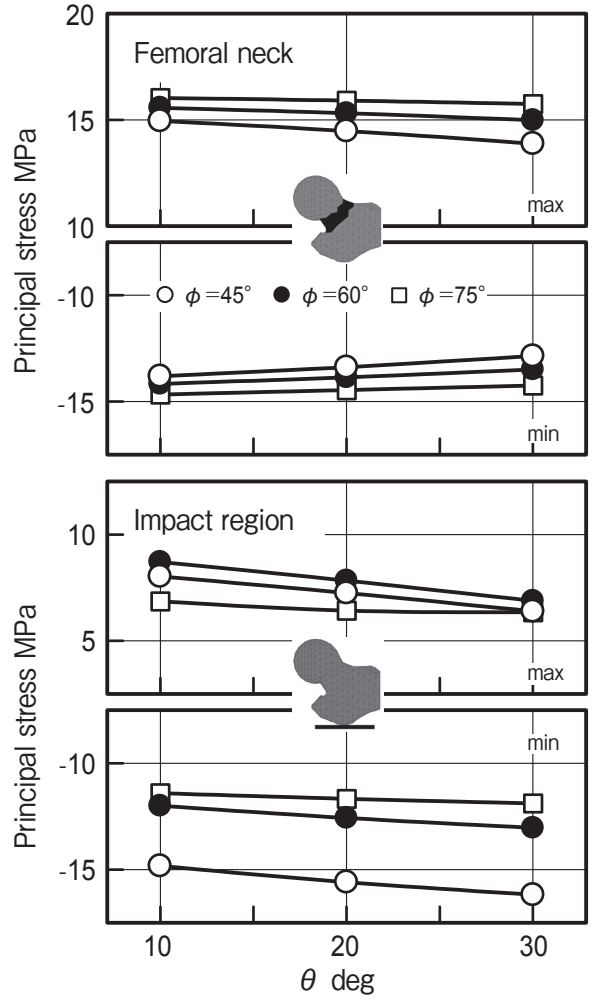

Fig. 9 The largest absolute values of the maximum and minimum principal stress in the femoral neck area and those in the impact region during the propagation of the stress wave (t = 0−500 μsec). The relation between the largest values and θ for each inclination angle is shown.

to the equivalent stress, the maximum principal stress on the medial side and the absolute value of the minimum one on the lateral side were large till t = 260 μsec, and the opposite state of the principal stress was observed after t = 260 μsec, as seen in Fig. 7A. In the case of a sideways fall, the impact bending occurs due to the greater trochanter hitting a rigid surface. As a result, the stress on the lateral side is compressive and that on the medial side is tensile at the first step. After the stress wave reached around the neck, it appears to have reflected in a complex way at the cortical bone surface, such that the opposite type of stress wave propagated after t = 260 μsec. The impact is applied in the vertical direction at the greater trochanter, so that the absolute values of the maximum and minimum principal stress are larger on the medial and lateral sides than on the anterior and posterior sides of the neck. The large absolute value of the principal stress in the cortical bone, shown in Fig. 6, can be explained as generated by the impact bending and the high elastic modulus of the cortical bone.

The deformation of the femur during the impact loading can also be evaluated by the finite element analysis. The red lines in Fig. 10 show the shapes of the proximal femur at t = 100, 200, 300, 400 μsec in the case of θ = 20°, φ = 60° (the displacements of the nodes were extended 100-fold for purposes of comparison). The initial shape is also indicated by the black lines for comparison. The femoral head displaces downward, and then moves upward, resulting in the time histories of the principal stress in the femoral neck shown in Fig. 7A.

As shown in Fig. 9, the influence of the fall configuration on the principal stress was relatively small in the femoral neck. The influence on the minimum principal stress was remarkable in the impact region and the absolute value of the stress for φ = 45° was larger than that for the other cases. This was due to the difference in the position of the greater trochanter upon impact, since the position in the case of φ = 45° was different from that in the cases of φ = 60 and 75 degrees. The absolute values of the maximum and minimum principal stress in the neck were nearly equal, and these values were close to the largest absolute value of the minimum principal stress in the impact region. The large absolute value of the compressive stress was found a little earlier in the impact region than in the neck at the beginning of the propagation, as shown in Fig. 7, indicating that the greater trochanter is at risk of fracture when the stress is larger than the bone strength. According to the reference [17], the tensile strength of the bone is generally lower than the compressive strength; thus bone fracture may occur on the medial or the lateral side of the neck even if it does not occur in the trochanter. These results will of course be affected by the shape of the individual femur, but this influence should not be very large, provided the shape is not highly different from that of the model used in the analysis.

In our previous paper [15], the impulsive stress

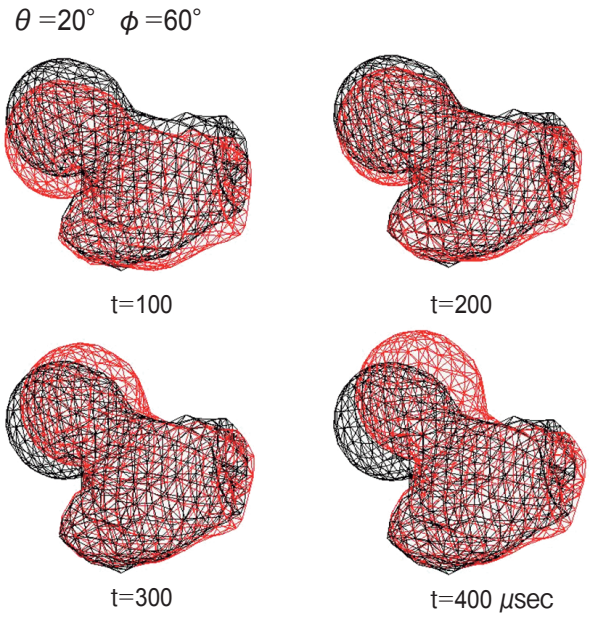

Fig. 10 Deformation of the proximal femur during the impact loading in the case of $\theta = 20°$, $\phi = 60°$. Displacements of the nodes were extended 100-fold for purposes of comparison. The shapes of the proximal femur at t = 100, 200, 300, 400 μsec are indicated with red lines and the initial shape is also shown using black lines for comparison.

waves propagating from the distal end of the femur were studied and it was clarified that the femoral neck and the trochanter are at risk of bone fracture when the impact is applied in the direction of the bone axis. For our present analysis, we set the impact velocity to be equal to that used in the previous study. The largest maximum principal stress obtained in the present study was 1.5 times larger than that obtained in the previous one. It follows that the application of this impact load to the greater trochanter would lead to a higher risk of bone fracture than the impact at the distal end of the femur; a sideways fall can thus cause a serious femoral fracture when the impact velocity is no greater than that generated by walking or going up and down stairs.

References

1. Yosibash Z, Padan R, Joskowicz L and Milgrom C: A CT-Based High-Order Finite Element Analysis of the Human Proximal Femur Compared to In-vitro Experiments. J Biomech Eng (2007) 129: 297–309.
2. Langton CM, Pisharody S and Keyak JH: Comparison of 3D finite element analysis derived stiffness and BMD to determine the failure load of the excised proximal femur. Med Eng Phys (2009) 31: 668–672.
3. Trabelsi N, Yosibash Z and Milgrom C: Validation of subject-specific automated p-FE analysis of the proximal femur. J Biomech (2009) 42: 234–241.
4. Bessho M, Ohnishi I, Matsumoto T, Ohashi S, Matsuyama J, Tobita K, Kaneko M and Nakamura K: Prediction of proximal femur strength using a CT-based nonlinear finite element method: Differences in predicted fracture load and site with changing load and boundary conditions. Bone (2009) 45: 226–231.
5. Yang H, Ma X and Guo T: Some factors that affect the comparison between isotropic and orthotropic inhomogeneous finite element material models of femur. Med Eng Phys (2010) 32: 553–560.
6. Trabelsi N, Yosibash Z, Wutte C, Augat P and Eberle S: Patient-specific finite element analysis of the human femur – A double-blinded biomechanical validation. J Biomech (2011) 44: 1666–1672.
7. Trabelsi N and Yosibash Z: Patient-Specific Finite-Element Analyses of the Proximal Femur with Orthotropic Material Properties Validated by Experiments. J Biomech Eng (2011) 133: 061001-1–061001-11.
8. Hambli R, Bettamer A and Allaoui S: Finite element prediction of proximal femur fracture pattern based on orthotropic behaviour law coupled to quasi-brittle damage. Med Eng Phys (2012) 34: 202–210.
9. Tsouknidas A, Anagnostidis K, Maliaris G and Michailidis N: Fracture risk in the femoral hip region: A finite element analysis supported experimental approach. J Biomech (2012) 45: 1959–1964.
10. Verim Ö, Taşgetiren S, Er MS, Timur M and Yuran AF: Anatomical comparison and evaluation of human proximal femurs modeling via different devices and FEM analysis. Int J Med Robotics Comput Assist Surg (2013) 9: e19–e24.
11. HAMBLI R and ALLAOUI S: A Robust 3D Finite Element Simulation of Human Proximal Femur Progressive Fracture Under Stance Load with Experimental Validation. Ann Biomed Eng (2013) 41: 2515–2527.
12. Nishiyama KK, Gilchrist S, Guy P, Cripton P and Boyd SK: Proximal femur bone strength estimated by a computationally fast finite element analysis in a sideways fall configuration. J Biomech (2013) 46: 1231–1236.
13. Eberle S, Göttlinger M and Augat P: Individual density-elasticity relationships improve accuracy of subject-specific finite element models of human femurs. J Biomech (2013) 46: 2152–2157.
14. Dall'Ara E, Luisier B, Schmidt R, Kainberger F, Zysset P and Pahr D: A nonlinear QCT-based finite element model validation study for the human femur tested in two configurations in vitro. Bone (2013) 52: 27–38.
15. Sarai T, Inoue T, Fujiwara K and Kuramoto K: Dynamic Finite Element Analysis of Impulsive Stress Waves Propagating from Distal End of Femur. Acta Med Okayama (2012) 66: 409–415.
16. Data Book on Mechanical Properties of Living Cells, Tissues, and Organs, Abé H, Hayashi K and Sato M eds, Springer-Verlag, Tokyo (1996): pp292–349.
17. Fung YC: Biomechanics - Mechanical Properties of Living Tissues, 2nd Ed. Springer-Verlag, New York (1993): pp510–513.